REPORT DOCUMENTATION PAGE

Form Approved
OMB No. 0704-0188

1. REPORT DATE *(DD-MM-YYYY)*
23-05-2006

2. REPORT TYPE
Technical Paper

3. DATES COVERED *(From - To)*

4. TITLE AND SUBTITLE

Comparison of Hall Thruster Plume Expansion Model with Experimental Data (Preprint)

5a. CONTRACT NUMBER

5b. GRANT NUMBER

5c. PROGRAM ELEMENT NUMBER

6. AUTHOR(S)

Carrie S. Niemela (Spiral Technology); Shannon Y. Cheng, Lubos Brieda, & Michael Nakles (ERC); Jared Ekholm & William Hargus, Jr. (AFRL/PRSS)

5d. PROJECT NUMBER
48470052

5e. TASK NUMBER

5f. WORK UNIT NUMBER

7. PERFORMING ORGANIZATION NAME(S) AND ADDRESS(ES)

Air Force Research Laboratory (AFMC)
AFRL/PRSS
1 Ara Drive
Edwards AFB CA 93524-7013

8. PERFORMING ORGANIZATION REPORT NUMBER

AFRL-PR-ED-TP-2006-155

9. SPONSORING / MONITORING AGENCY NAME(S) AND ADDRESS(ES)

Air Force Research Laboratory (AFMC)
AFRL/PRS
5 Pollux Drive
Edwards AFB CA 93524-70448

10. SPONSOR/MONITOR'S ACRONYM(S)

11. SPONSOR/MONITOR'S NUMBER(S)
AFRL-PR-ED-TP-2006-155

12. DISTRIBUTION / AVAILABILITY STATEMENT

Approved for public release; distribution unlimited (AFRL-ERS-PAS-2006-123)

13. SUPPLEMENTARY NOTES

Presented at the 42nd AIAA/ASME/SAE/ASEE Joint Propulsion Conference, Sacramento, CA, 9-12 July 2006.

14. ABSTRACT

Numerical modeling of the expansion of electric thruster plumes provides direct means for predicting spacecraft surface contamination and erosion due to plume ions. A software package named COLISEUM that is capable of self-consistently modeling plasma propagation and interactions with arbitrary 3-D surfaces is being developed by a national team of researchers. Despite much research and development in modeling plume expansion, it is necessary to continuously validate these codes using laboratory based experimental data. It is well-established that vacuum chamber facilities affect the plume of these devices. Thus, the models must not only describe the plume expansion, but also effects of the vacuum chamber. COLISEUM has been designed to simulate both vacuum chamber configurations and spacecraft geometries. This work provides source derivation from laser induced florescence (LIF) data. Included is a study that compares results from a hybrid particle-in-cell model (AQUILA) with Monte Carlo collisions to data obtained from the plume of Busek 600W Hall thruster (BHT-HD-600). This data includes current density, velocity distribution, and energy data.

15. SUBJECT TERMS

16. SECURITY CLASSIFICATION OF:			17. LIMITATION OF ABSTRACT	18. NUMBER OF PAGES	19a. NAME OF RESPONSIBLE PERSON
a. REPORT	**b. ABSTRACT**	**c. THIS PAGE**			Daron Bromaghim
Unclassified	**Unclassified**	**Unclassified**	A	19	**19b. TELEPHONE NUMBER** *(include area code)* N/A

AIAA-2005-4480

Comparison of Hall Thruster Plume Expansion Model with Experimental Data (Pre-print)

Carrie S. Niemela*
Spiral Technology, Inc. Air Force Research Laboratory, Edwards AFB, CA 93536

Shannon Y. Cheng†, Lubos Brieda‡, and Michael R. Nakles§
ERC, Inc., Air Force Research Laboratory, Edwards AFB, CA 93536

and

Jared M. Ekholm**, William A. Hargus, Jr.++
Air Force Research Laboratory, Edwards AFB, CA 93524

Numerical modeling of the expansion of electric thruster plumes provides direct means for predicting spacecraft surface contamination and erosion due to plume ions. A software package named COLISEUM that is capable of self-consistently modeling plasma propagation and interactions with arbitrary 3-D surfaces is being developed by a national team of researchers. Despite much research and development in modeling plume expansion, it is necessary to continuously validate these codes using laboratory based experimental data. It is well-established that vacuum chamber facilities affect the plume of these devices. Thus, the models must not only describe the plume expansion, but also effects of the vacuum chamber. COLISEUM has been designed to simulate both vacuum chamber configurations and spacecraft geometries. This work provides source derivation from laser induced florescence (LIF) data. Included is a study that compares results from a hybrid particle-in-cell model (AQUILA) with Monte Carlo collisions to data obtained from the plume of Busek 600W Hall thruster (BHT-HD-600). This data includes current density, velocity distribution, and energy data.

I. Introduction

Numerical modeling of the thruster and surrounding environment provides direct means for predicting plume properties where experimental methods are limited, such as predictions of spacecraft interactions. Insight into the plume properties and corresponding spacecraft interaction would provide the community with a useful tool. The Air Force Research Laboratory (AFRL) is leading the development of COLISEUM[1], a 3D plasma interaction framework that incorporates a plasma expansion tool with surface interactions. COLISEUM has been designed to be usable, flexible, and expandable. COLISEUM has available any of four plasma simulation models, RAY, *prescribed_plume*, DRACO, and AQUILA. RAY uses a ray-tracing method to project a flux from a point surface. *Prescribed_plume* imports and superimposes a plume distribution onto surfaces. DRACO tracks particles along a structured Cartesian mesh. AQUILA, the focus of this study, is a hybrid PIC model that tracks particles along an unstructured tetrahedral mesh. COLISEUM is capable of modeling chamber effects, which are known to affect the plume expansion[2], as well as open boundary conditions.

* Research Engineer, Spiral Technology, Inc., 1 Ara Road Edwards AFB, CA 93536, Member AIAA.
† Research Engineer, ERC, Inc., 1 Ara Road Edwards AFB, CA 93536, Member AIAA.
‡ Research Engineer, ERC, Inc., 1 Ara Road Edwards AFB, CA 93536, Member AIAA.
§ Research Engineer, ERC, Inc., 1 Ara Road Edwards AFB, CA 93536, Member AIAA
** Research Scientist, AFRL/PRSS, 1 Ara Road Edwards AFB, CA 93536, Member AIAA
++ Research Engineer, AFRL/PRSS, 1 Ara Road Edwards AFB, CA 93536, Senior Member AIAA

Despite much research and development in modeling plume expansion,[3,4,5,6] it is necessary to continuously validate these codes using laboratory based experimental data. This paper presents a study that compares results from an AQUILA simulation to experimental data from the BHT-HD-600 Hall thruster. The numerical study uses a simplified Hall thruster to simulate an electric plume in a chamber environment. Laser induced florescence (LIF) data is used to construct source input files. Probes in AQUILA collect current density, velocity distributions, and ion velocities which are compared to experimental data for code validation. The full capabilities of AQUILA are expressed by using probes to collect additional information about the plume.

II. AQUILA code

AQUILA, a hybrid particle-in-cell model, has been developed in the framework of COLISEUM. AQUILA uses an unstructured tetrahedral mesh to define surface and volume geometries. The geometry and mesh used by COLISEUM can be produced using available commercial modeling and meshing packages. The mesh can be loaded into COLISEUM using any number of standard forms including ANSYS and ABAQUS. Individual surfaces are specified to distinguish surface properties and define particle/surface interactions.

In most places of the plume, the plasma is defined to be quasi-neutral. Following this assumption, the potential can be calculated by using the inverted Boltzmann equation:

$$\phi = \phi_o + \frac{kT_e}{e}\ln\left(\frac{n_e}{n_{eo}}\right)$$

where n_{eo} is a reference ion density, ϕ_o is a reference electrostatic potential, and T_e is the reference electron temperature. For plumes where the quasi-neutral assumption does not hold, such as behind a plume shield, AQUILA contains a non-neutral solver.[3]

Collisions are performed in AQUILA[7] using a Direct Simulation Monte Carlo method[8]. Collision cross sections for elastic collisions[9] between neutrals and ions are calculated using:

$$\sigma^{el}_{Xe-Xe} = \frac{2.117x10^{-18}}{v_{rel}^{0.24}}$$

$$\sigma^{el}_{Xe-Xe^{+}} = \sigma^{el}_{Xe-Xe^{++}} = \frac{8.2807x10^{-16}}{v_{rel}}$$

where v_{rel} is the relative velocity between the two particles. Charge exchange collision cross sections between ions and neutrals[10] are defined as:

$$\sigma^{CEX}_{Xe-Xe^{+}} = 2.2415x10^{-18} - 2.7661x10^{-19}\log(v_{rel})$$

$$\sigma^{CEX}_{Xe-Xe^{++}} = 1x10^{-20}(35.006 - 2.7038\log(v_{rel}))^2$$

The current density probe in AQUILA samples particles on a hemisphere at a user defined location. The results along the hemisphere are averaged to give values from 0 to 90º.

To decrease computational time, acceleration techniques have been introduced into AQUILA. One of the acceleration techniques utilizes a subcycle routine that decouples the ion and neutral movements. This method has been demonstrated previously[1]. Subcycling cycles the fast particles for a specified time step before moving and injecting the slow particles and performing collisions. Subcycling in AQUILA is shown to decrease the computational time for the simulation to reach steady state by 77%, as shown by Marshall and VanGilder[11].

However, it is also shown that too many subcycles (~100) allow an ion to leave the main region of the plume without undergoing any collisions, an event that may not be entirely physical.

III. Source Definition

Plasma modeling within COLISEUM begins with source definition. Sources are used to introduce particles into the simulation domain. COLISEUM provides several different source models, all specifying a velocity distribution function (VDF) and a mass flow rate. While several source models are available, the test case used in this paper used the source FLUX_R_VZ_VR[12]. As the name suggests, the FLUX_R_VZ_VR model represents the exit plane of a Hall thruster in terms of:

1. particle flux versus radial position, r
2. axial velocity, v_z, versus radial position, r
3. radial velocity, v_r, versus radial position, r

Before starting the simulation run, the flux function is converted into a cumulative distribution function for radial position. During injection of particles, the simulation uses the thruster's mass flow rate to determine the number of particles to create at each time step. The previously-computed cumulative distribution function (CDF) is then used to place source particles at radial distances with the correct probability. Once the radial location of the injected particle is known, the initial velocity components are calculated from the velocity functions. In addition, thermal components are added to these velocities based on user-specified temperatures.

Laser-induced florescence data provides a natural way of determining the VDF required by the simulation source model. After processing, the data taken at each location gives a probability distribution function of the velocity component aligned with the laser used to probe the plasma. To get velocity distribution functions along a different axis, the orientation of the laser is changed. For this source model, all VDF inputs were taken from LIF data[13] at an axial distance of 15 mm downstream from the thruster exit plane. Figure 1 shows the geometry of the BHT-HD-600.

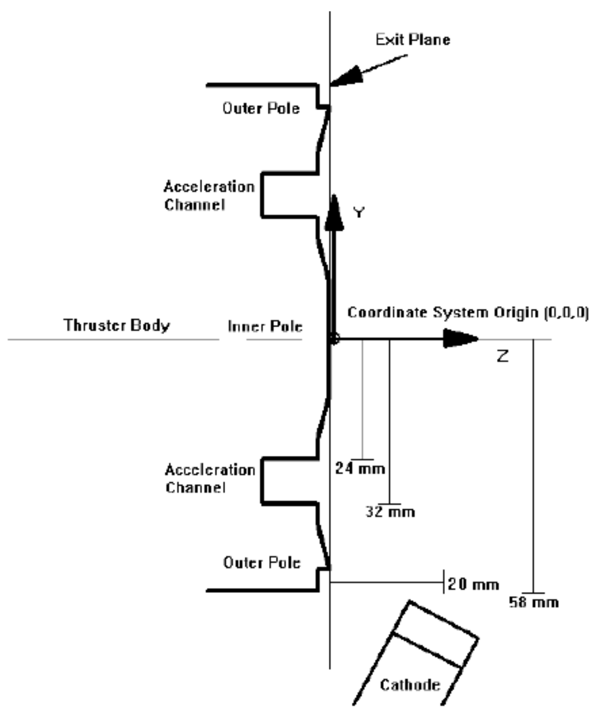

Figure 1: BHT-HD-600 geometry for LIF analysis. The data for the LIF analysis is taken at y = 15 mm which is between the exit plane of the thruster and the cathode.

A. Velocity Distributions

Figure 2 shows a representative axial VDF for the BHT-HD-600 taken at a radial distance of 24 mm from the centerline. A distinct velocity peak is seen around 20,000 m/s. To quantify the mean and spread of the peak, the velocity distribution function is converted to a histogram and a Matlab function that fits a specified number of Gaussians is used. Figure 3 illustrates this process – the red lines show the fitted Gaussians. In most cases, two Gaussians were used to fit the histogram – one captures the property of the peak of interest while the other represents background noise in the signal.

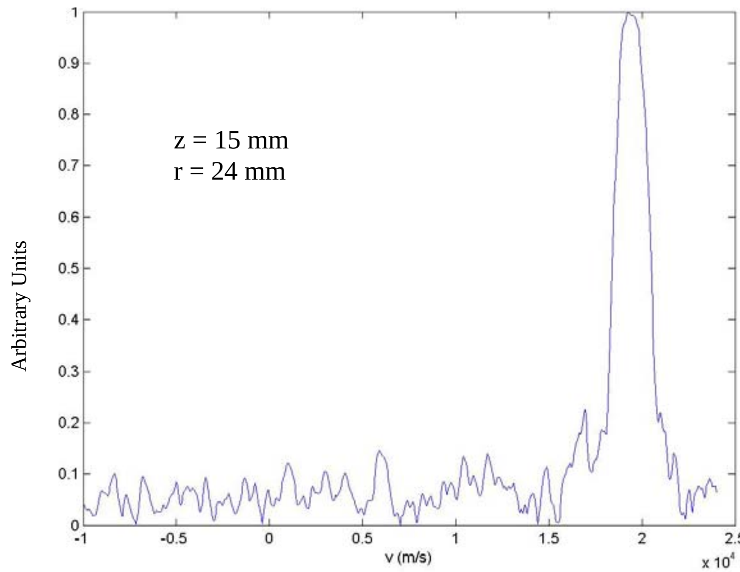

Figure 2: Axial velocity distribution function at r = 24mm of BHT-HD-600.

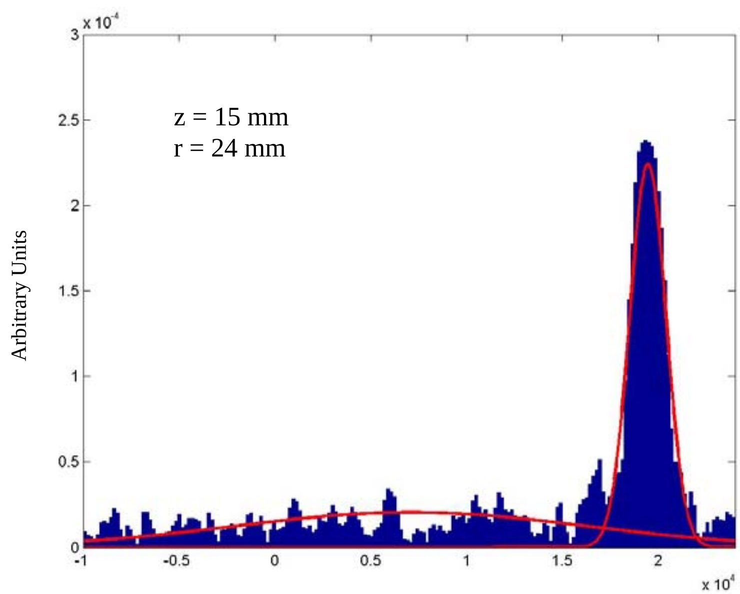

Figure 3: Histogram with fitted Gaussians for axial velocity distribution function at r = 24 mm.

A similar procedure is followed at each radial location with LIF data for both the axial and radial velocity components. The mean of the main Gaussian is used to represent the velocity magnitude, while the standard deviation is used to represent the temperature. Since the source model assures azimuthally symmetry, only values from one side of the thruster are needed – for this case, values from the non-cathode side of the thruster are taken

Upon further inspection of the LIF data, it is observed that evidence of a second ion population is seen in the axial velocity distribution functions found on the cathode side of the thruster. Compared to the above figures, Figure 4 shows the corresponding axial distribution at r = 24 mm on the cathode side.

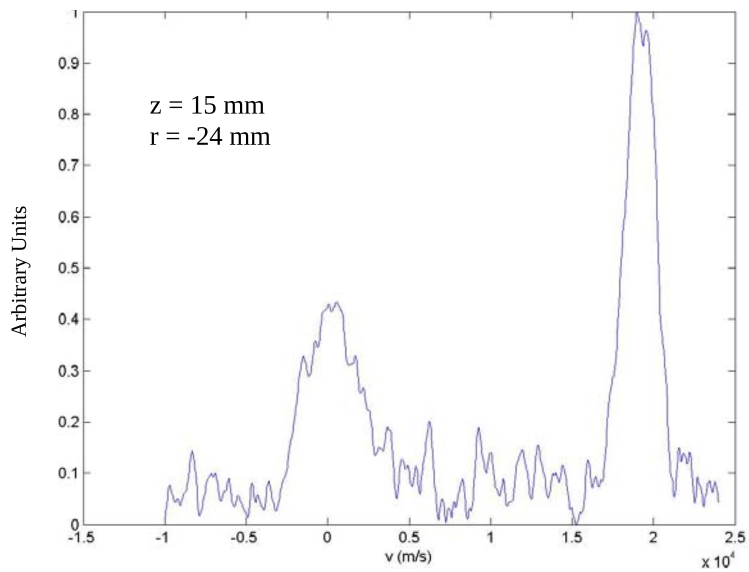

Figure 4: Axial velocity distribution function at r = -24mm (cathode side) of BHT-HD-600.

Two defined axial velocity peaks are observed, but when the radial distributions are investigated, no difference in behavior is seen. It is conjectured that the second axial peak on the cathode side may be related to additional ionization that occurs near the exit plane. Electrons streaming from the cathode are assumed uniformly azimuthally distributed by the magnetic field once they enter the thruster acceleration channel and as a result, ionization is also uniform. However, neutrals outside the thruster on the cathode side are more susceptible to ionization by electrons before they reach the channel. Since these ions are formed outside of the main accelerating potential, their existence is manifested by a smaller lower-energy peak in the axial distributions. As currently written, the AQUILA source model cannot model an asymmetric exit plane distribution. Nevertheless, source model information including this second population is also processed in case one considers the second low-energy peak important.

B. Flux Distribution

Flux measurements for the BHT-HD-600 have not yet been completed. An attempt was made to extract ion flux data from LIF signal strength. Signal strength in the linear regime is proportional to both ion density at the probed state and to the intensity of the beam[14]. This approximation holds if the ion and electron temperatures and the electron density are relatively constant throughout the region. The peak signal strength at each data location for z = 15 mm is plotted as single points in Figure 5. Using a curve fitting algorithm, a Gaussian profile was fit to this data. The flux profile shifts the center of the distribution away from the centerline of the channel (at r = -28 mm) towards the center line of the thruster (r = 24 mm). An input file was generated using this distribution.

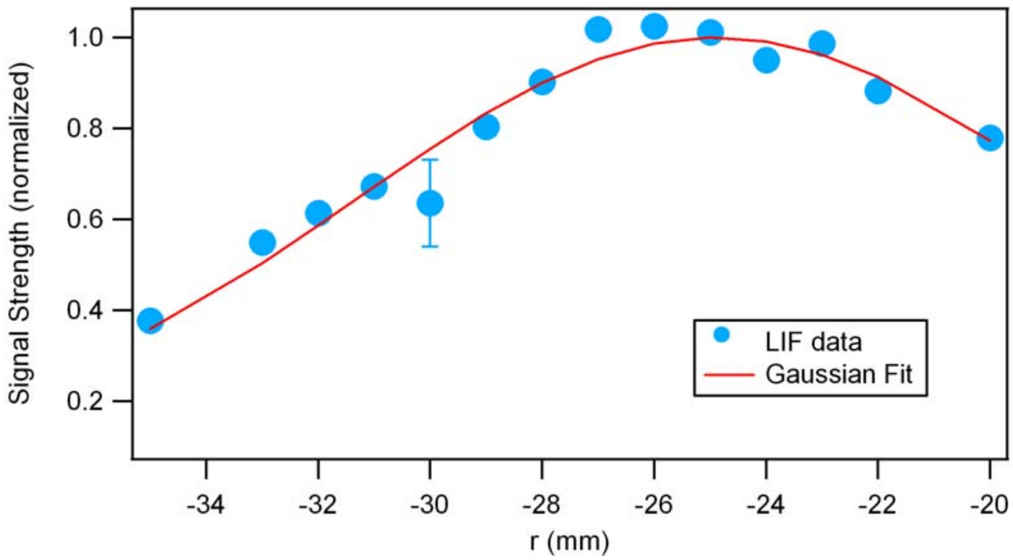

Figure 5: Flux profile generated from LIF signal strength data fitted with a Gaussian distribution. The Gaussian fit to the LIF data is centered at r = -24 mm rather than over the centerline of the thruster at r = -28 mm.

IV. Problem Description

The chamber and thruster geometry for the simulations is based on the BHT-HD-600 Hall thruster live tests inside Chamber 6 at the Air Force Research Laboratory. During the thruster testing, graphite panels were added to the chamber to lower sputter rates of the chamber and reduce re-deposition of the chamber materials back onto the thruster. The simulation preserved the placement and orientation of the graphite panels while simplifying the geometry of the panels and other components to increase mesh quality. Figure 6 shows the surface mesh of the chamber, graphite panels, and thruster orientation. The thruster fires in the negative z direction.

The chamber modeled is a 1.8 m diameter, 2.9 m length stainless steel chamber. The graphite panels are modeled as semi-circular shapes concentric with the chamber, 60 cm in width and lengths from 79 cm to 1.22 m. Cryogenic pumps are also included in the geometry at the rear of the chamber, 87 cm wide and 83 cm apart. The chamber background pressure was set to 7×10^{-4}, corrected for Xe.

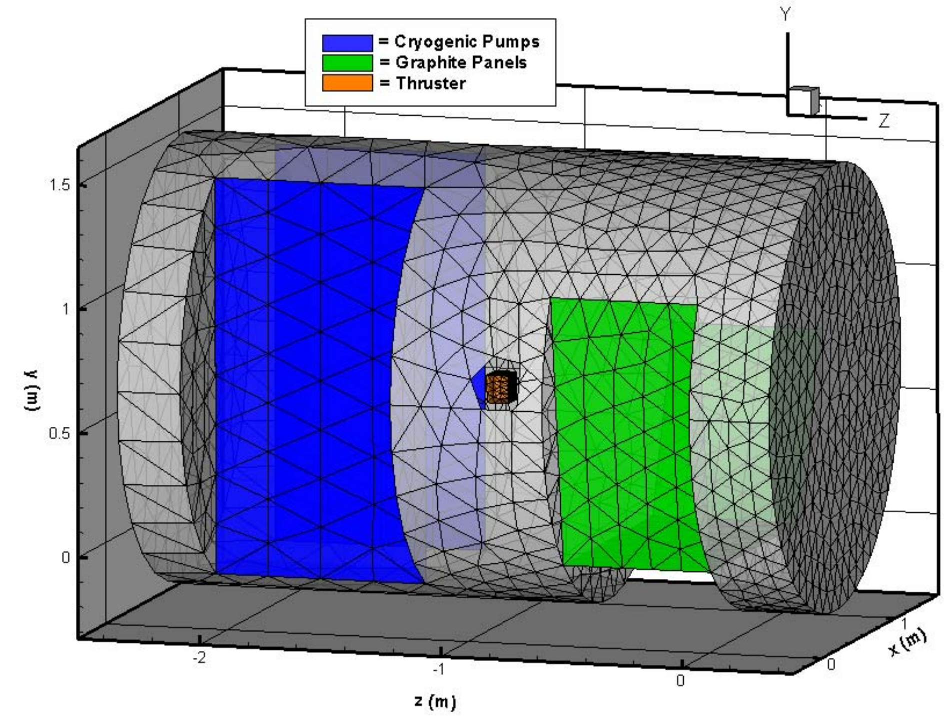

Figure 6: Chamber 6 geometry and mesh. The green elements are the graphite panels. The blue elements are the cryogenic pumps. The thruster is the orange box in the center of the chamber.

The simulated Hall thruster geometry, shown in Figure 7, is the plasma emitting source in the simulation. Particles are emitted from the annular region of the thruster face. Based on the geometry of the BHT-HD-600, the annulus has an inner diameter of 24 mm and an outer diameter of 32 mm.

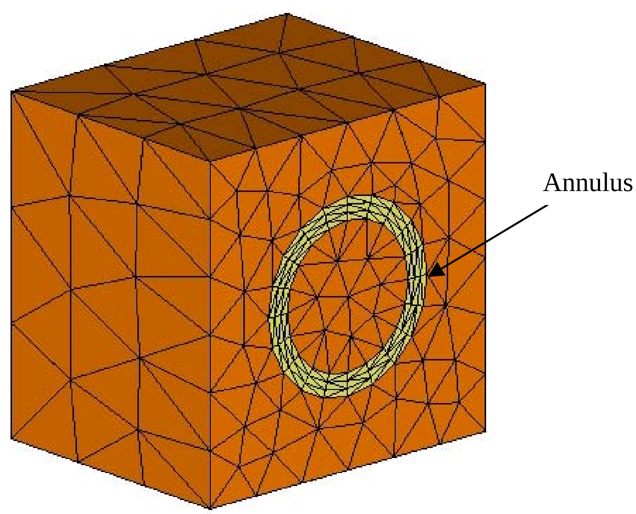

Figure 7: BHT-HD-600 simplified mesh. The yellow elements are defined as the particle emitting source. Notice the change in element resolution from the front face to the back.

The volume mesh used in this simulation is shown in Figure 8. The mesh is a structured mesh in the core region of the plume, produced to increase/control the resolution of elements in the immediate region of the plume. This region is defined by the annulus extending outward 30 cm from the thruster face, with the end elements triple the size of the original elements. An unstructured mesh fills in the remainder of the volume.

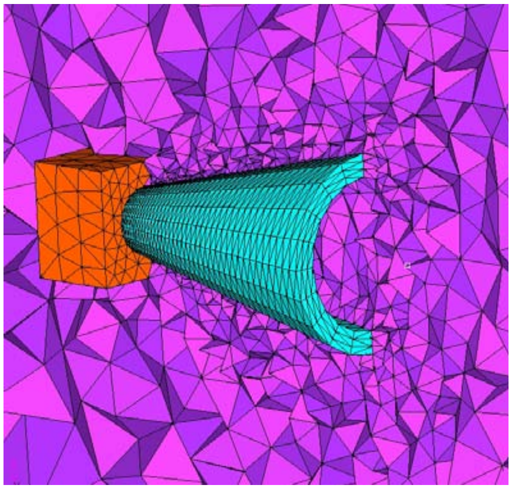

Figure 8: The simulated volume mesh with a structured mesh in the region of the plume and an unstructured mesh in the remaining volume. The structured mesh is used to control the resolution of the mesh in the immediate region of the plume.

The annular region, shown in Figure 7, is the particle emitting source of the simulation. Based on experimental findings[15], the particles emitted include not only Xe neutrals and singly charged Xe ions, but multiply charged Xe ions as well. The distribution of neutrals is defined by a drifting Maxwellian source model with a thermal drift velocity of 297 m/s and a temperature of 700 K. The mass flow rate of neutral particles into the simulation reflects 10% of the unionized propellant. Source files for doubly charged ions were generated using the singly charged ion source files, increasing the magnitude of velocity by the √2 to represent an increase in speed related to their charge according to the energy relation:

$$\frac{1}{2}mv^2 = Zq\phi$$

where Z is the ion charge, q is the elementary charge, and ϕ is the potential.

Although evidence of a low velocity ion population was seen in the axial LIF data, this population was only evidenced in the cathode region of the plume. Since the majority of the plume lacks this second population, the simulation was completed using only the main population of ions, and the flux profile shown in Figure 5. Ion temperatures of 10 eV in the radial, axial, and azimuthal directions were used.

The electrostatic potential uses the quasi-neutral potential solver in AQUILA. The reference potential ϕ_o is set to 20 eV, and the reference density n_{eo} is sampled from the domain at a point centered on the annular channel. The ion temperature T is specified using a polytropic model:

$$T = T_e\left(\frac{n_e}{n_{eo}}\right)^{\gamma-1}$$

where the reference electron temperature T_e is set to 5.0 eV and γ is 1.3.

The timing scheme in AQUILA is used to determine when the simulation reaches a steady state. Subcycling was used in this simulation to decrease computation time. The number of subcycles was set at 10, with an ion time step of 2×10^{-7} s, and the number of cycles was 2500. The region of the domain specified as the cryogenic pumps takes incoming particles out of the domain at a user specified rate. To determine correct cryogenic pumping speed for the simulation, the neutral count should reach a steady state when the source ions begin to collide with the wall. Using a time step of 2×10^{-7} s, source ions reach the wall in 7.5×10^{-5} s. During the simulation, this occurs after 39 cycles. Running the simulation with various cryogenic sticking coefficients, it is shown that this is achieved at a pumping speed of 8%. Figure 9 shows the particle count plot for neutrals.

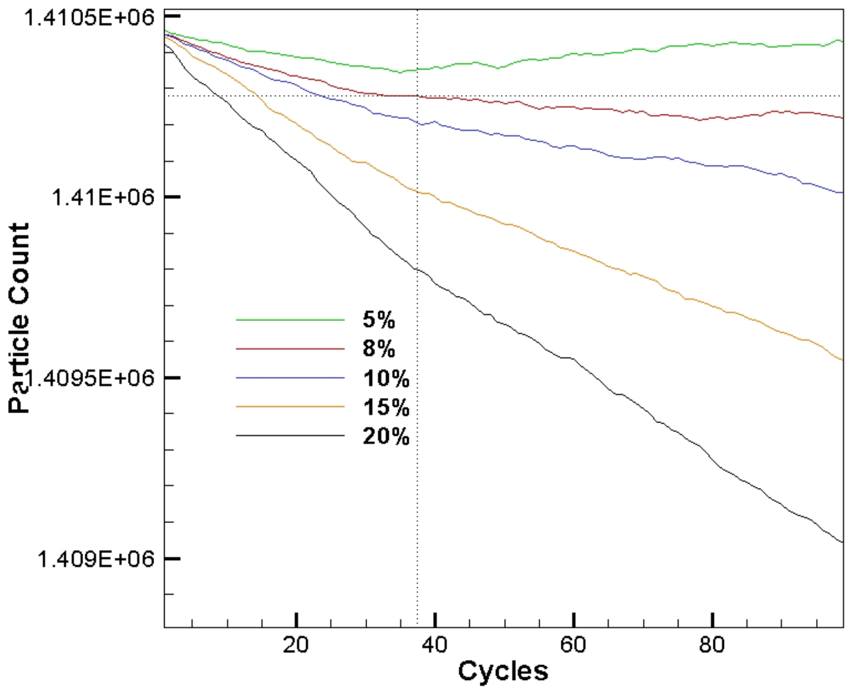

Figure 9: Neutral particle count for different sticking coefficients. An adequate sticking coefficient of 8% is indicated by a level neutral count after 39 cycles, when source ions begin to collide with the wall.

V. Comparison against Experimental Data

The plume studies of the BHT-HD-600 conducted by Ekholm, et al[15], provided measurements of the ion current density profile, ion energy distributions, and ion species fraction distributions using a nude Faraday probe, retarding potential analyzer (RPA), and ExB probe. LIF measurements were taken from Charles and Hargus[13]. This suite of data serves as a comparison to the test cases completed using AQUILA and the input parameters defined above.

A. Current Density

The current density probe in AQUILA was set up to sample particles along a hemisphere 60 cm in front of the thruster, allocating 200 bins for sampling. Figure 10 shows the current density from the test case compared to experimental results from Faraday probe measurements at 60 cm. As shown in Figure 10, the trend in the current density profile agrees with experimental data across the region, although the magnitudes only agree from -20º to 20º. In the wing region of the plume, the data for the test case is lower than what is seen experimentally. Experiments are known to have difficulties in this region due to charge exchange collisions and secondary electron emission from ion impact with the probe. The difference could also indicate greater collision rates in the plume than what is modeled. Increasing collision rates would lead to greater plume divergence and spread more ions out towards the wings. Despite the differences, the similar trend between the two sets of data suggests that only minor refinements are needed in the model to bring the both sets of data into agreement.

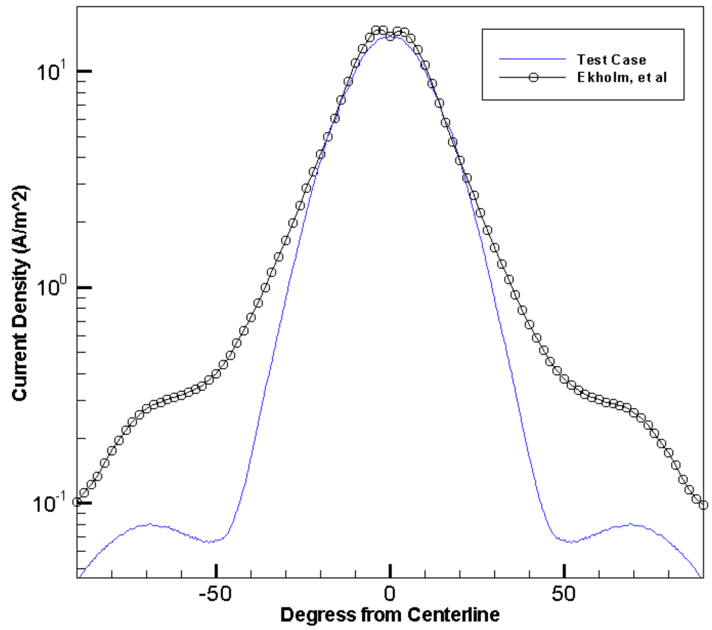

Figure 10: Current density at 60 cm from Ekholm, et al and from test case. The trends in both sets of data are similar, with the greatest differences occurring in the wings of the plume from -40º to 40º. Greater collision rates in the model would broaden the spread of the test case profile.

B. Near Field Ion Velocities

Figure 11 shows a comparison of axial ion velocities at x = 0 mm, z = 60 mm from the thruster exit with LIF peak data values taken by Charles and Hargus and an uncertainty of 500 m/s. Figure 12 is the radial velocity comparison in this same region. AQUILA tracks particles based on the collisions they undergo and attaches a prefix to the species name. An SRC delimiter signifies a beam ion that has not experienced any collisions. EL_COL and CEX_COL label ions that have undergone elastic and charge exchange collisions, respectively. It can be noted that the trend of the simulated source ions follows the trend of the LIF data, with the axial velocities around 20 km/s and a 3 km/s deep depression around y = 0 mm. The radial velocities follow a linear pattern across both sections of the channel, changing from a divergent to convergent profile at y = +-30 mm, noted by a shift in velocities from positive to negative. As is expected, the ions undergoing collisions are shown to have axial velocities around 1000 m/s and radial velocities near 0 m/s. There is also a significant amount of distribution in the velocity which is seen in data taken by Charles and Hargus. While the greatest population of ions occurs at the peak, higher velocity and lower velocity populations exist. Figures 11 and 12 suggest that the model portrays consistent results in the near-field as compared to experimental data.

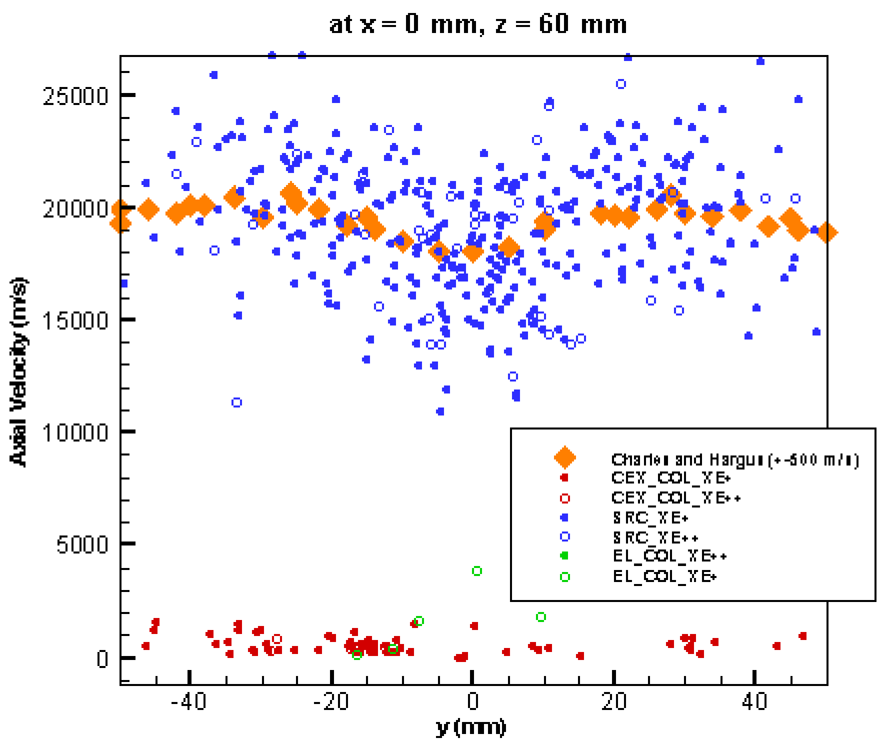

Figure 11: Axial LIF comparison at 60 mm in front of thruster. The trends from both the experimental and test case data agree, with a significant amount of distribution in the test case data also seen in the data by Charles and Hargus.

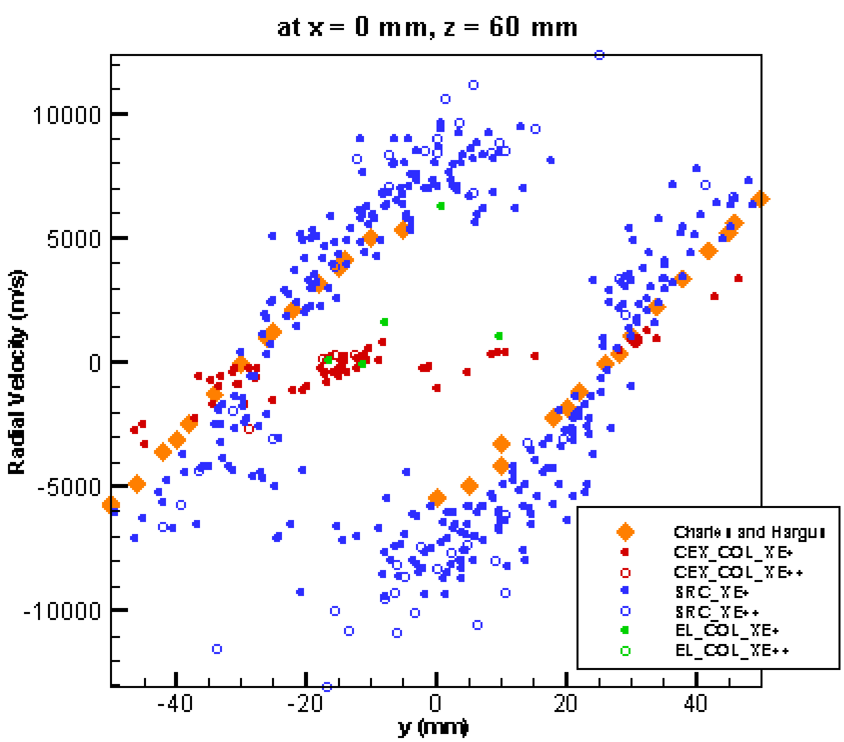

Figure 12: Radial LIF comparison at 60 mm in front of the thruster. The trends from both the experimental and test case data agree, with a significant amount of distribution in the test case data also seen in the data by Charles and Hargus.

C. Far Field Energy Distribution

The energy distribution of ions in the simulation can be determined from the ion velocities. Using the equation for kinetic energy: KE = ½ mv^2, with the mass of a Xe ion as 2.182 $x10^{-25}$ kg, the kinetic energy per charge is computed along an arc 60 cm in front of the thruster in the x-z plane. The resulting plot is shown in Figure 11, compared against RPA experimental data. The RPA probe measures an energy distribution per charge; the peak values are shown in Figure 11, along with a bar representing the distribution spread seen in the data, around 10% of the peak value. The same particle labels are used in Figure 13 as in Figure 11 and 12. As is expected, collision ions are shown to have energies between 0 and 50 eV/q, with some elastic scattering seen around 100 to 150 eV. It is interesting to note that Ekholm, et al noticed a peak in the RPA data in the 150 eV range, attributing it to elastic scattering. Beam singly charged ions have much higher energies, with a mean value near 325 eV/q and a broad distribution from 150 eV/q to 550 eV/q that falls outside the range of experimental data. The doubly charged beam ions have the same amount of energy as their singly charged counterparts, but because of their double charge, their energy per charge is only half. Notice that the beam ions reside only in the region between -40º to 40º, suggesting a low beam divergence. The combination of a large range of ion energies and mean value higher than the peak experimental results suggests that the source may be emitting particles at velocities that are too high and/or over too great a range. By adjusting the thermal component of the velocity, it is possible to confine the velocity range and bring the model energy values to a more reasonable level. The near field results suggest that the source model velocities are consistent with experimental LIF data, although the far field results indicate that the particle velocities are too high. This suggests that there may be an issue in the far field that needs to be addressed, including mesh resolution, potential solver parameters, collision properties, and background pressure.

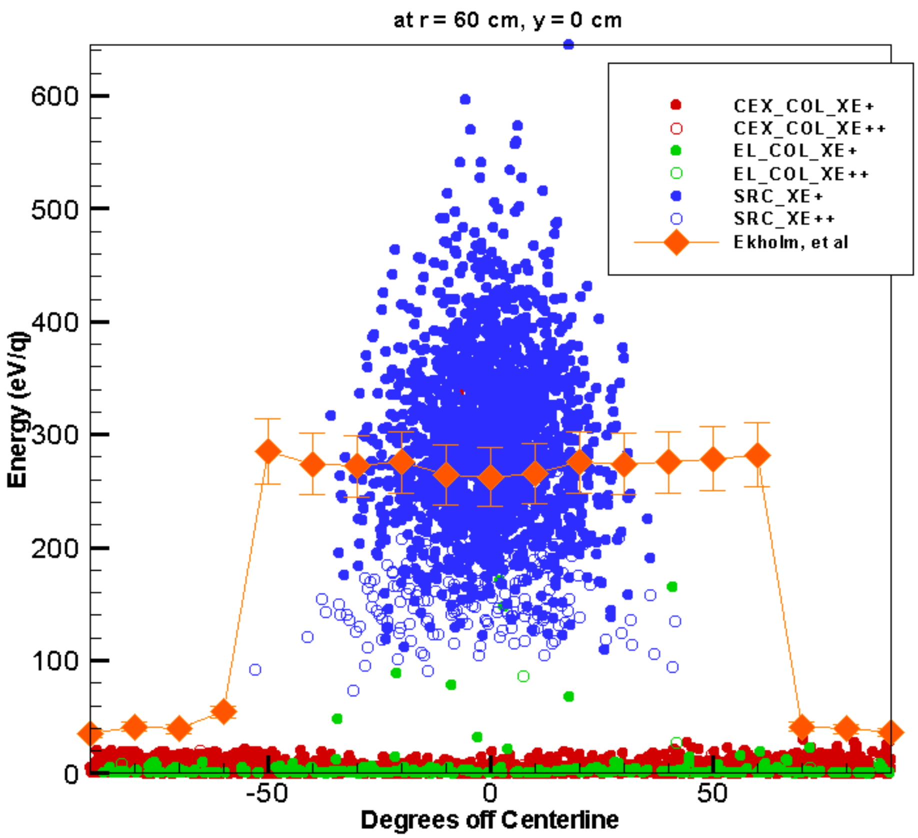

Figure 13: Ion Energy Distribution at r = 60 cm from Ekholm, et al and from the test case. The ions are labeled according to the collisions they experience. EL_COL and CEX_COL denote elastic collisions and charge exchange collisions respectively. SRC symbolizes beam ions that have not undergone any collisions. The energy distribution for beam ions is between 150 eV and 550 eV, with a mean value around 325 eV. This suggests a liberal thermal component that requires additional investigation.

VI. Results

Computer models provide an insight into the less tangible characteristics of the plume. Using the test case above, plots were constructed for several properties including potential, ion temperature, ion density, and Debye length. These plots are shown in Figures 14-21 in both a full chamber perspective and a close up view of the thruster. Potential plots are shown in Figures 14 and 15. As is predicted, the greatest potential (24 V) is seen directly in front of the thruster, expanding radially outwards and decreasing with increasing distance from the thruster. In the detail view, the potential contours converge along the thruster centerline a distance out from the thruster face. Ion temperatures, shown in Figures 16 and 17 follow the same trend, with a maximum temperature of 5 eV directly in front of the thruster. Ion density, illustrated in Figures 18 and 19 show the highest concentration of ions ($3.6 \times 10^{17}/m^3$) directly in front of the thruster, dropping off rapidly outside the immediate region of the plume. Debye length is shown in Figures 20 and 21. The Debye length inside the chamber drops from 2.6×10^{-5} in front of the thruster to 8×10^{-6} at the back of the chamber.

VII. Conclusion

This particular test case has shown that the results from AQUILA agree with experimental data in magnitude and trend while not always agreeing in distributions. Results from near-field velocity profiles indicate that the source model velocity distributions are consistent with experimental data, although results from the far field energy distributions suggest that the thermal component may need additional investigation. The comparisons against current density and energy distribution indicate a narrow beam divergence, possibly caused by low collision rates. Far field energy profiles also suggest additional investigation into far field model parameters, such as mesh refinement. Future work needs to be completed in AQUILA to determine which parameters effectively decide beam divergence, control velocity distributions, and far field properties.

VIII. Future Work

The simulation was completed using only one, optimal test case. The results indicate that adjustments to the collision rates, ion temperature distribution, and far field properties may yield more accurate results. Also, by changing other parameters of the simulation such as background pressure, mesh quality, and potential solver inputs, the results from the simulation could change. A sensitivity analysis of AQUILA to input parameters is of future interest. In addition, more data from the BHT-HD-600 may become available in the future. At that time, it would be pertinent to compare the data to results from this model.

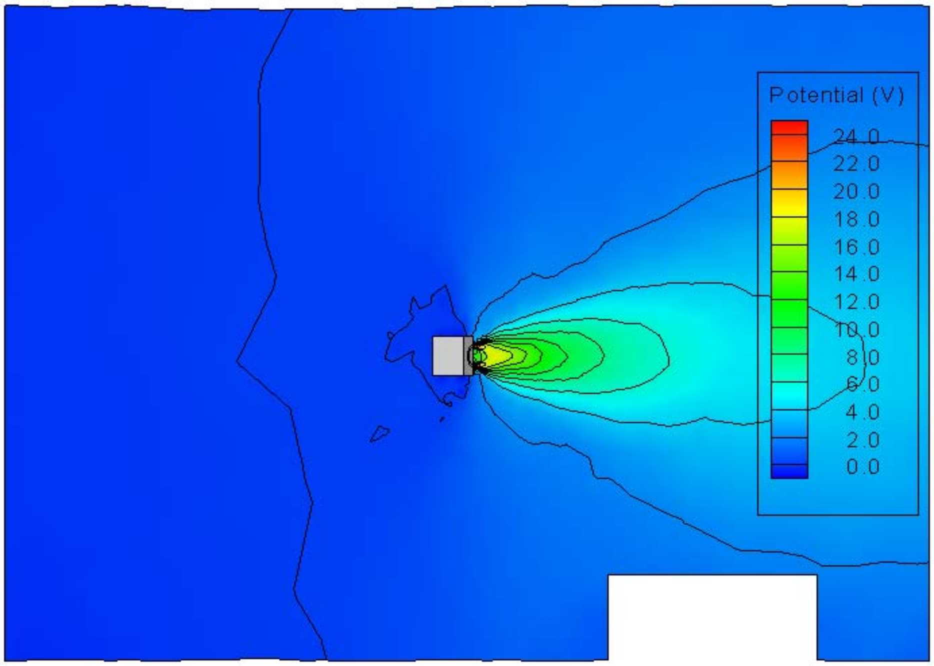

Figure 14: Chamber view of electrostatic potential. The potential profile diverges radially outward in the main region of the beam, decreasing in magnitude from 24 V to 0 V at the back of the chamber.

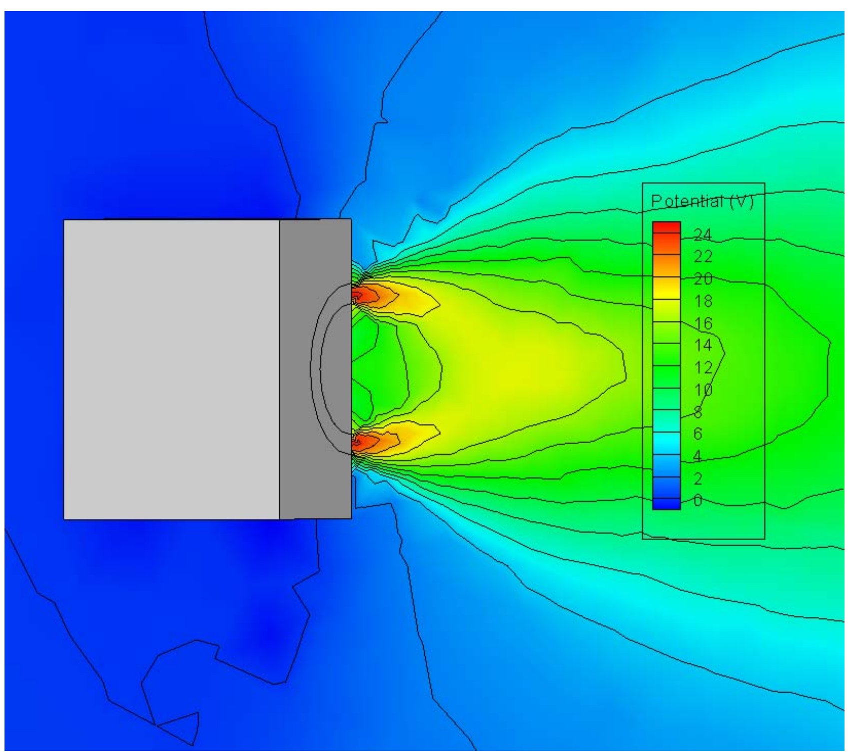

Figure 15: Thruster view of electrostatic potential. The potential quickly drops off from 24 V in front of the thruster and converges along the centerline of the thruster downstream.

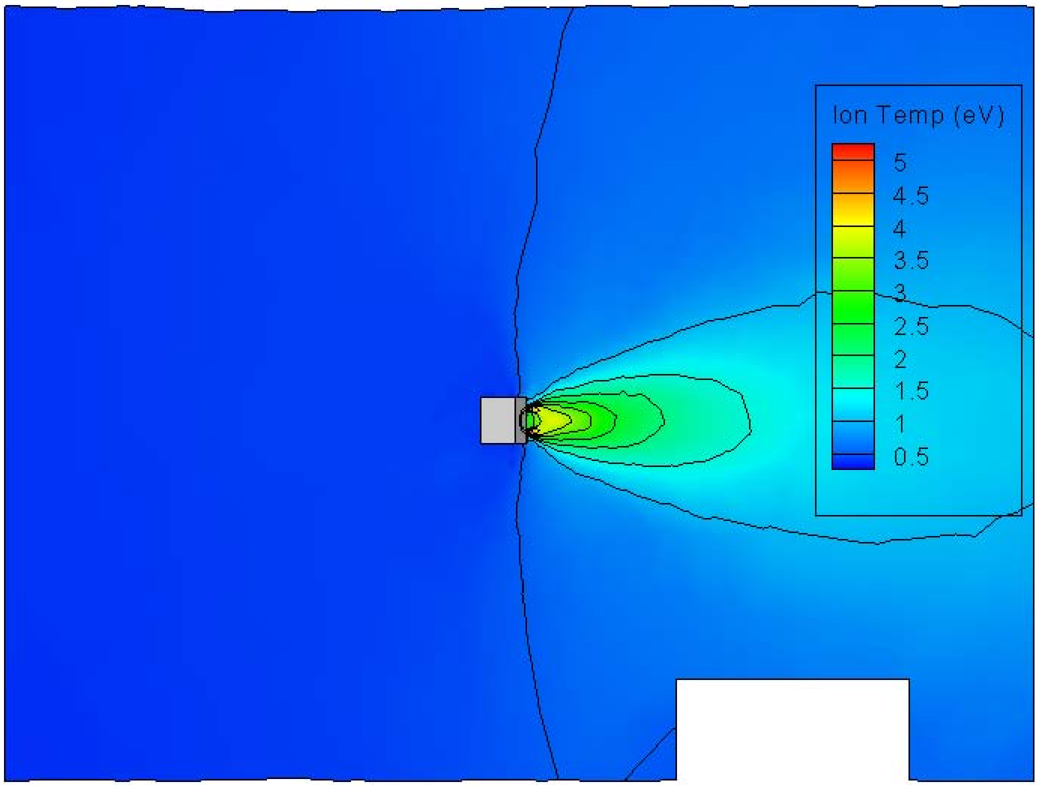

Figure 16: Chamber view of ion temperature. The temperature ranges from 5 eV in front of the thruster to 0.5 eV in the back of the chamber. The profile radiates outward following the same trend seen in the potential.

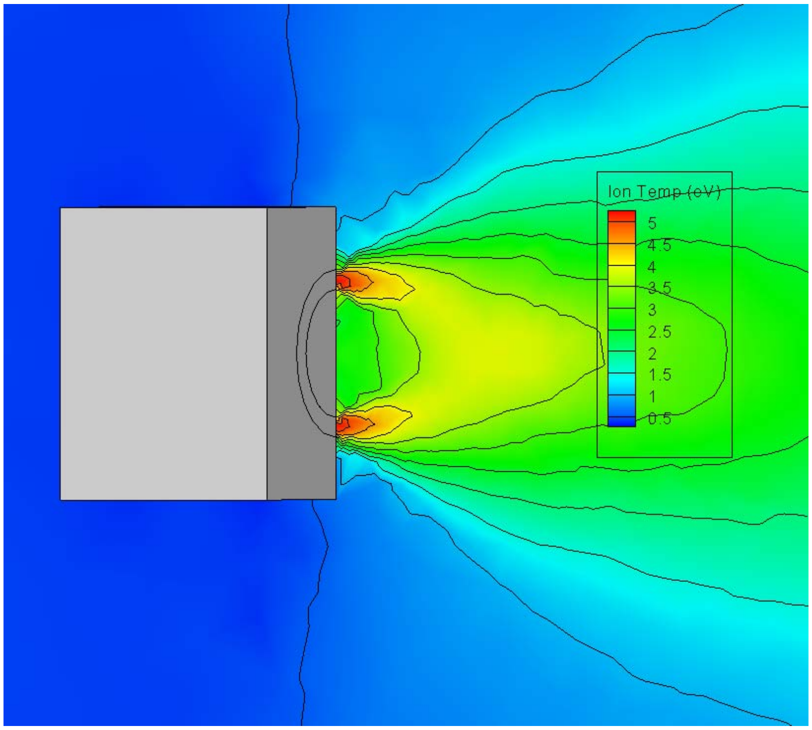

Figure 17: Thruster view of the beam ion temperature. The ion temperature matches the potential profile by converging along the centerline downstream of the thruster.

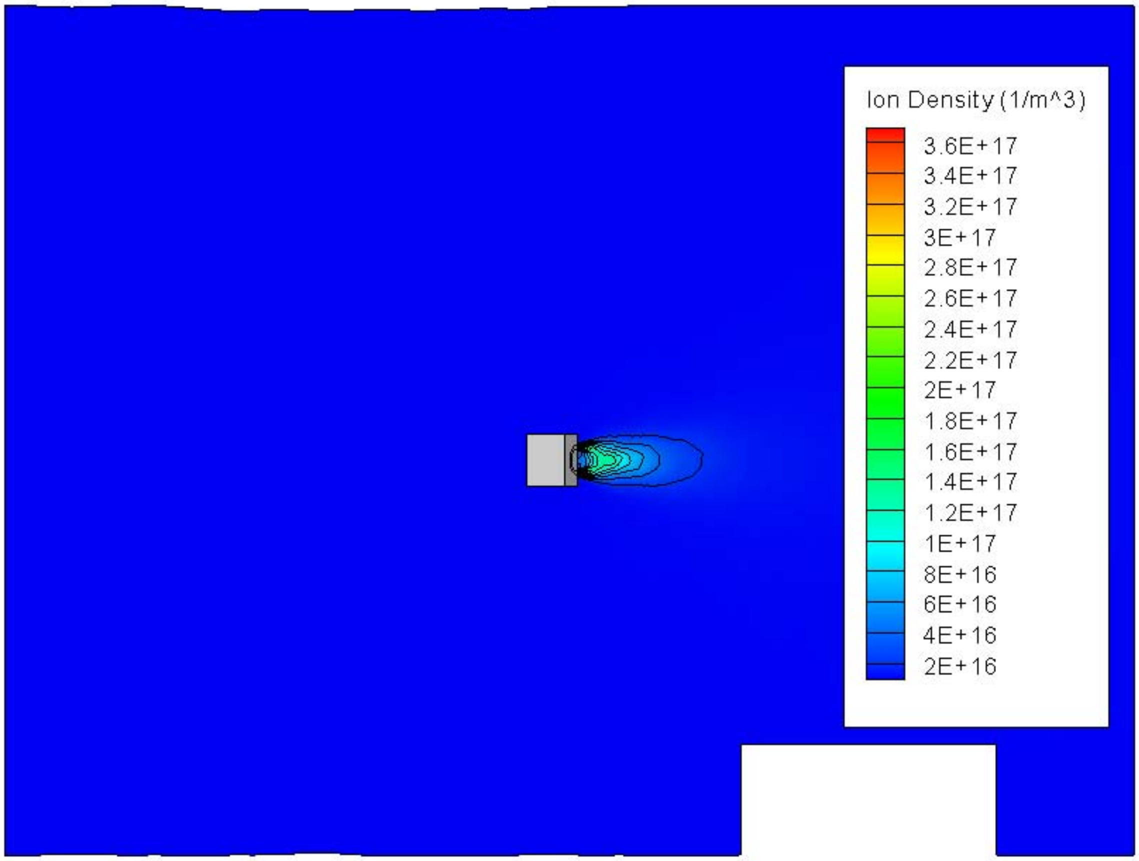

Figure 18: Chamber view of ion density. The greatest concentration of ion density is directly in front of the thruster. The ion density drops outside the main region of the plume to a background density of 2 x 10^{16}.

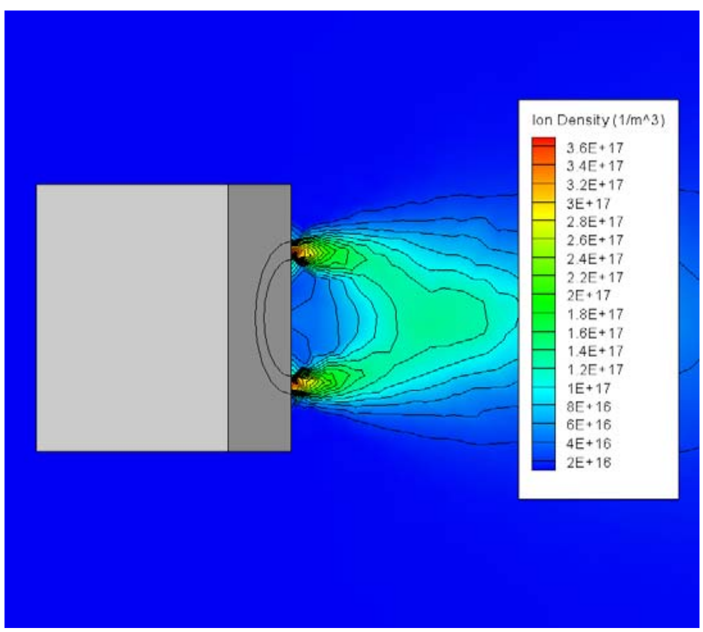

Figure 19: Thruster view of ion density. The ion density also converges on the centerline of the thruster, similar to the potential and ion temperature profiles as seen in Figures 15 and 17.

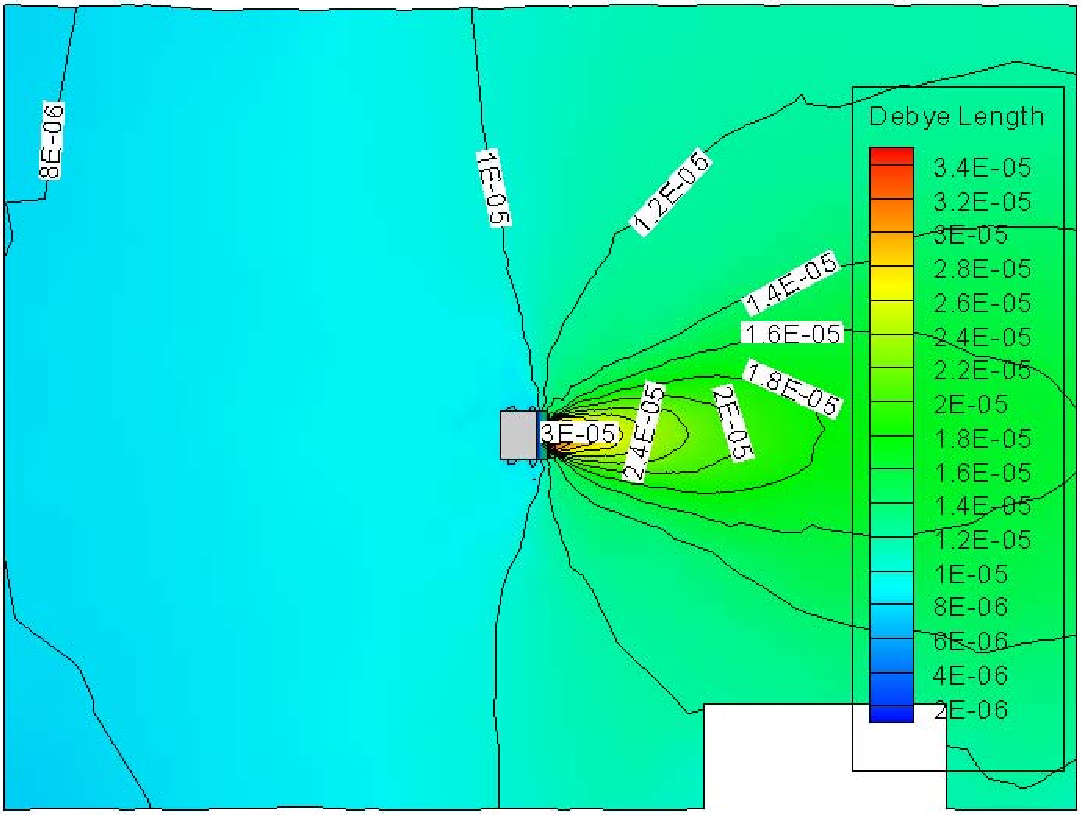

Figure 20: Chamber view of Debye length. The Debye length is 1.0 x 10^{-5} in the wings of the thruster and drops to 8 x 10^{-6} in the far reaches of the chamber.

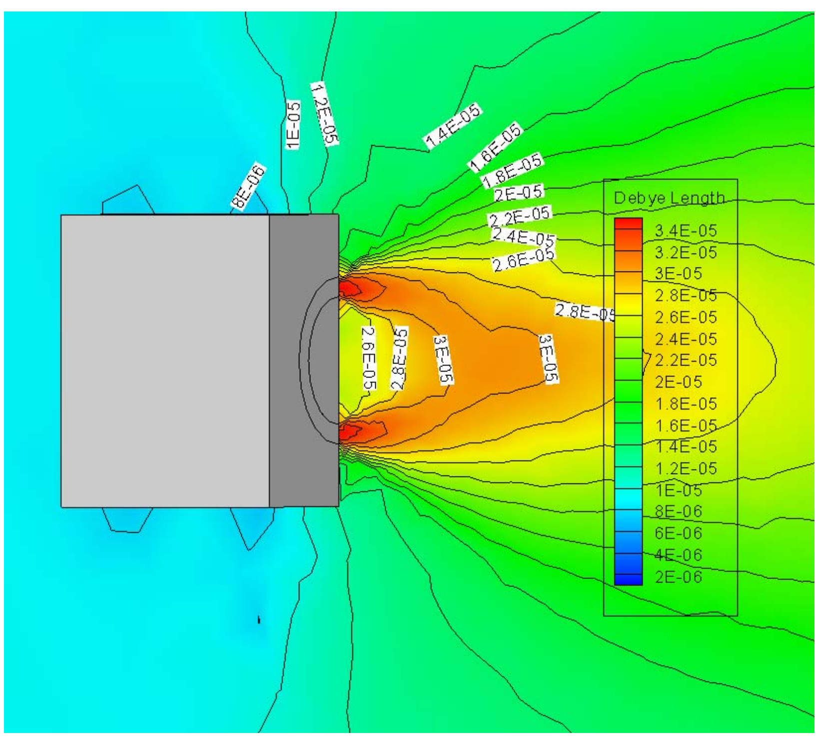

Figure 21: Thruster view of Debye length. The Debye length in the front of the thruster is 2.6 x 10^{-5} and 3 x 10^{-5} downstream, along the centerline of the thruster.

Acknowledgments

Thanks to Doug VanGilder, for his initial guidance and instruction in code implementation and collision modeling.

References

[1] Gibbons, M.R., Kirtley, D.E., VanGilder, D.E., Fife, J.M., "Flexible Three-Dimensional Modeling of Electric Thrusters in Vacuum Chambers," *39th AIAA/ASME/SAE/ASEE Joint Propulsion Conference*, AIAA-2003-4872.

[2] Randolph, T. et al., "Facility Effects on Stationary Plasma Thruster Testing," *23rd International Electric Propulsion Conference*, IEPC-93-093.

[3] Santi, M., Cheng, S., Celik, M., Martinez-Sanchez, M., and Peraire, J., "Further Development and Preliminary Results of the AQUILA Hall Thruster Plume Model," *39th AIAA/ASME/SAE/ASEE Joint Propulsion Conference*, AIAA-2003-4873.

[4] Brieda, L., Pierru, J., Kafafy, R., and Wang, J., "Development of the DRACO code for Modeling Electric Propulsion Plume Interactions," *40th AIAA/ASME/SAE/ASEE Joint Propulsion Conference*, AIAA-2004-3633.

[5] VanGilder, D.B. et al., "Particle Simulations of a Hall Thruster Plume," Journal of Spacecraft and Rockets, Vol.37 No.1.

[6] Oh, D. and Hastings, D., "Three Dimensional PIC-DSMC Simulations of Hall Thruster Plumes and Analysis for Realistic Spacecraft Configurations," *32nd AIAA/ASME/SAE/ASEE Joint Propulsion Conference*, AIAA-1996-3299.

[7] Celik, M., Santi, M., Cheng, S., Martinez-Sanchez, M. and Peraire, J., "Hybrid-PIC Simulation of a Hall Thruster Plume on an Unstructured Grid with DSMC Collisions," *28th International Electric Propulsion Conference*, March 17-20 2003.

[8] Bird, G.A., *Molecular Gas Dynamics and the Direct Simulation of Gas Flows*, Oxford University Press, Oxford, 1994.

[9] Oh, D. Y. and Hastings, D.E., "Experimental Verification of a PIC-DSMC Model for Hall Thruster Plumes," *32nd AIAA/ASME/SAE/ASEE Joint Propulsion Conference*, AIAA-1996-3196.

[10] Hasted, J.B. and Hussain, M. *Proc. Phys. Soc*. **83,** 911 (1964).

[11] Marshall, D.D., and VanGilder, D.B., "Investigation of Particle-in-Cell Acceleration Techniques for Plasma Simulations," *37th AIAA Plasmadynamics and Laser Conference*.

[12] Cheng, S.Y. and Martinez-Sanchez, M. "Comparison of Numerical Simulation to Hall Thruster Plume Shield Experiment," *40th AIAA/ASME/SAE/ASEE Joint Propulsion Conference*, AIAA-2004-3635.

[13] Charles, C.S. and Hargus, W.A., Personal Communication, Unpublished data from Laser Induced Fluorescence Velocity Measurements of a BHT-600 Hall Thruster.

[14] Hargus, W.A., and Nakles, M.R., "Evolution of the Ion Velocity Distribution in the Near Field of a 200W Hall Thruster," *42nd AIAA/ASEE/SAE/ASEE Joint Propulsion Conference*, AIAA-2005-4991.

[15] Ekholm, J. M., Hargus, W.A., Larson, C.W., Nakles, M.R., Reed, G., and Niemela, C.S., "Plume Characteristics of a 600W Hall Thruster," *42nd AIAA/ASME/SAE/ASEE Joint Propulsion Conference*.